Article

Journal of the Brazilian Chemical Society

https://dx.doi.org/10.21577/0103-5053.20240087

J. Braz. Chem. Soc. **2024**, *35*, 11, e-20240087, 1-15

Smart Solid Drug Delivery Systems: Exploring the pH Sensitivity of Cashew Gum-Doxorubicin Prodrug

Irisvan S. Ribeiro,[a] Adisom L. S. Leonardo,[a] Maria J. M. Carneiro,[a] Raimundo N. Costa Filho,[b] Rosemayre S. Freire,[b] Jeanlex S. Sousa,[b] Gisele S. Araújo,[c] José D. B. Marinho Filho,[c] Ana J. Araújo,[c] Haroldo C. B. Paula,[a] Judith P. A. Feitosa[*,a] and Regina C. M. de Paula[a]*

[a]*Laboratório de Polímeros, Departamento de Química Orgânica e Inorgânica, Centro de Ciências, Universidade Federal do Ceará, 60020-181 Fortaleza-CE, Brazil*

[b]*Departamento de Física, Centro de Ciências, Universidade Federal do Ceará, 60440-900 Fortaleza-CE, Brazil*

[c]*Laboratório de Cultura de Células do Delta, Universidade Federal do Delta do Parnaíba, 64202-020 Parnaíba-PI, Brazil*

Polysaccharide-based prodrugs formed via pH-responsive covalent interactions can be used to prepare nanoparticles for drug delivery to tumor cells. This study reports the synthesis of cashew gum-doxorubicin prodrugs via Schiff base (CG-S-DOX) and amide bonds (CG-A-DOX), both of which exhibit pH-responsive behavior. Synthesis was confirmed using spectroscopic techniques. Drug-binding content and efficiency were higher for CG-S-DOX than for CG-A-DOX. The capacity of the nanoparticles to self-organize in aqueous media was confirmed using fluorescence spectroscopy, dynamic light scattering, and atomic force microscopy. Both prodrugs possessed sizes < 200 nm and showed responsive doxorubicin-release profiles in the acidic tumor cell microenvironment. Compared with free DOX, the CG-S-DOX and CG-A-DOX prodrug had significantly reduced cytotoxicity against non-tumor cells (L929). CG-S-DOX, but not CG-A-DOX, showed antitumor activity against HCT-116 (human colorectal cancer) and MCF-7 (human breast cancer) cells. An uptake assay confirmed that the nanoparticles were easily taken up by HCT-116 cells. These results together with the great reduction in cytotoxicity against non-tumor cells, confirm the potential of CG-S-DOX prodrug nanoparticles as a reliable and efficient system for the effective delivery of doxorubicin to tumor cells.

Keywords: cashew gum, Schiff base, conjugates, cancer, pH responsive

Introduction

Prodrugs are formed via stimulus-responsive covalent bonds between a desired drug and other molecules, such as antibodies, peptides, polymers, and inorganic nanoparticles.[1,2] Prodrug delivery platforms can decrease cytotoxicity in normal tissues and improve drug bioavailability. Because they accumulate in target cells, drugs can be activated by internal cellular stimuli, such as acidity, enzymes, and reactive oxygen species, or by external stimuli, such as light, temperature, and ultrasound, thereby increasing their toxicity in the desired microenvironment.[1,2] Prodrugs are stable during extracellular transport and respond to changes in the target cellular microenvironment, enabling controlled drug release or activation at the target site.

Polymeric prodrugs (polymer-drug conjugates) with pH-responsive covalent bonds have been investigated for enhanced drug release at targeted sites (cancer cells), owing to the acidic microenvironment of tumor cells and tissues.[3-5] The extracellular tumor microenvironment (pH 6.5-6.8) is more acidic than that in normal tissues (pH 7.2-7.4), due to the Warburg effect (aerobic glycolysis in tumor cells), likely because cancer cells exhibit increased production of lactic acid from glucose.[6] In addition, the intracellular tumor microenvironment (early endosomes: pH 5.9-6.2; late endosomes and lysosomes: pH 5.0-5.5) has lower pH than the extracellular tumor microenvironment.[7]

*e-mail: judith@dqoi.ufc.br
Editor handled this article: Célia M. Ronconi (Associate)

The conjugation between a hydrophilic polymer and hydrophobic drug offers several advantages, such as: (*i*) spontaneous formation of nanoparticles via self-assembly in water;[8] (*ii*) improved water solubility of hydrophobic drugs;[9] (*iii*) prolonged drug circulation in the blood plasma;[10] (*iv*) improved selective drug release to cancer cells (controlled by pH, redox capacity, and/or temperature);[11] (*v*) reduced drug toxicity against healthy cells, tissues, and organs;[12] and (*vi*) amplification of drug absorption by tumor tissues via the enhanced permeability and retention (EPR) effect.[13]

Polysaccharides have been studied as matrices for polysaccharide-drug conjugates, because they are biocompatible and nontoxic. Additionally, they contain various functional groups (hydroxyl, amino, and carboxyl groups) that can be exploited for synthesizing prodrugs via covalent bonds, such as amide,[14] boronate,[15] ester,[16] hydrazone,[17] and imine[18] bonds that are sensitive to the tumor microenvironment.

Cashew gum (CG), a natural, nontoxic, and biocompatible polysaccharide has been used to develop carbon quantum dots,[19] biosensors for catechol and bacteria detection[20,21] and coacervates as a food ingredient.[22] It has also been used as excipient in tablet formulations,[23] in bioactive films for wound dressing applications,[24] and in drug delivery systems as a promising agent against cancer,[25] neglected diseases,[26,27] inflammatory bowel disease,[28] and Chagas disease.[29] In addition, chemical modifications of CG, such as aldehyde (CHO) groups, can expand its range of applications and have been used to develop scaffolds for tissue engineering.[30,31]

The composition and structure of CG from Brazilian sources have been previously investigated. Studies by de Paula *et al*.[32] and Menestrina *et al*.[33] showed that the structure is mainly composed of branched galactose residues, linked at C-1 and C-3 (main chain), C-1 and C-6, and C-1, C-3, and C-6. Other monosaccharides (glucose, arabinose, uronic acid, and rhamnose) are present as small side chains or at the terminal position.

Oxidation of polysaccharides by sodium periodate has been used since early polysaccharide chemistry as a strategy for structural characterizations (Smith degradation).[34] Insertion of dialdehyde groups into the polysaccharide structure can increase chain flexibility, enhance biodegradability,[34] and potentially provide a strategy for new polysaccharide-based materials via Schiff base formation through reaction with amine groups.[35] Oxidation by sodium periodate is selective and only occurs if the OH groups in the monosaccharide units are vicinal and assume an equatorial-equatorial or equatorial-axial orientation.[36]

The World Health Organization's International Agency for Research on Cancer (IARC) counted almost 20 million people of both sexes who had cancer in 2022 worldwide. Mortality in the same year was almost 10 million. The incidence in Brazil in the same year was more than 600 thousand, with just under 300 thousand deaths. IARC estimated that between 2022 and 2045 the incidence of cancer will grow by 63.4%, while the population should only grow by 20.0%, with the increase in the number of cancers growing more than 3 times that of the population. In Brazil, the situation seems more serious, as it is estimated that the incidence of cancer will grow more than 9 times that of the population in the same period. The situation regarding mortality will be further worsened with the mortality rate rising to almost 80% in 2045, when in 2022 it was around 50%.[37] Obviously, the accuracy of the estimate will depend on studies on new and more effective technologies to combat cancer.

Doxorubicin (DOX) is an anti-neoplastic drug classified as anthracyclines, routinely used in the treatment of various cancers, such as liver,[38] breast,[39,40] and leukemia.[41] It has shown also promising results against several other types of cancer, including melanoma,[42] prostate,[43] ovarian,[44] and lung.[45] Unfortunately, clinical application of DOX is currently limited because of its high cytotoxicity to normal tissues and cells and limited water solubility.[46] Furthermore, this medication causes several side effects, such as inhibition of deoxyribonucleic acid (DNA) replication in normal cells, cardiotoxicity[40] and also alopecia, vomiting, leukopenia and stomatitis.[41]

To reduce these undesired effects, some therapies involving nanotechnology have been proposed. Caged xanthones, thiosemicarbazones derivatives and photosensitizers were explored as new drug candidates with alternative mechanisms of action.[39] Thermoresponsive polymeric DOX nanocarrier based on cholesterol and poly(*N*-isopropylacrylamide) showed high efficacy against breast cancer cells and good compatibility with normal cells.[40] PEGylated (PEG: polyethylene glycol) multi walled carbon nanotubes have been identified as an efficient pH dependent DOX carrier.[41] Superparamagnetic nanoparticles were proposed as a multiplatform for controlled release of DOX, and work as a chemo-hyperthermia nanodevice.[47] Magnetic pH-triggered DOX-polydopamine prodrug showed *in vivo* liver tumor inhibition and was indicated as potential for cancer treatment.[38] Mesoporous silica nanoparticles functionalized with carboxylate groups, containing DOX and capped by quaternary ammonium pillar[5]arene nanogates demonstrated *in vitro* ability to penetrate and release DOX into the nucleus of human breast adenocarcinoma cancer cells (MCF-7), inducing a pronounced cytotoxic effect.[48]

The present study reports the synthesis of pH-responsive CG-DOX prodrugs as potential nanocarriers, to overcome the aforementioned disadvantages and offer new perspectives for cancer treatment. Several polysaccharides have been studied as matrices for DOX prodrugs.[7,10-12] However, polysaccharides derived from exudate trees, such as cashew gum, have not yet been explored for this purpose. Due to their high solubility and branched structure, they could significantly influence the properties of DOX, including loading content, drug release kinetics, as well as physicochemical characteristics like particle size and zeta potential.

Two prodrugs were synthesized; the first was obtained via Schiff base reaction between the CHO group of oxidized CG and the amino group of DOX (CG-S-DOX), forming an imine bond. Reduction of the imine bond to an amine bond led to the formation of a second prodrug system (CG-A-DOX). The synthesis involves CG, an abundant, low cost, and biocompatible polysaccharide from Brazilian biodiversity, and its effects on cancer cells. Cytotoxicity in HCT-116 (human colorectal cancer), MCF-7 (human breast cancer), and L929 (murine fibroblast non-tumor) cells and cellular uptake efficiency were also evaluated.

Experimental

Materials

The cashew exudate was provided by Embrapa Agroindústria Tropical (Fortaleza City, Ceará, Brazil). CG was isolated and purified according to a protocol developed by our group.[49] The CG used in this study had an average molar mass of 3.4×10^4 g mol^{-1}, as determined by size exclusion chromatography using a refractive index detector, with a molar sugar ratio of 1.00:0.20:0.08:0.05:0.06 for galactose:glucose:arabinose:rhamnose:glucuronic acid. DOX hydrochloride (DOX·HCl), sodium periodate ($NaIO_4$), sodium borohydride ($NaBH_4$), and triethylamine were purchased from Merck (Brazil). Dimethyl sulfoxide (DMSO), hydroxylamine hydrochloride (NH_2OH·HCl), ethylene glycol, ethanol P.A., and acetone P.A. were obtained from Synth (Brazil). The DMSO was dried using a molecular sieve prior to synthesis.

CG oxidation

CG oxidation was performed as described by Maciel *et al.*[30] The molar ratio CG (5.0 g, 3.09×10^{-2} mol of glycosidic units) was dissolved in distilled water (100 mL) for 24 h. After complete dissolution, 0.66 g of $NaIO_4$ (3.09×10^{-3} mol) was added to obtain CG with 10% of the units oxidized. The reaction mixture was stirred at 25 °C for 24 h in the dark and the reaction was terminated by adding ethylene glycol (170 µL). The resulting dispersion was dialyzed in a cellulose membrane (molecular weight cut-off 14 kDa) against distilled water until the conductivity of the dialysis water was equal to that of distilled water (5 days) and then freeze-dried to obtain a white flocculent solid, denoted as OCG. The degree of oxidation was determined using the hydroxylamine hydrochloride/sodium hydroxide (NH_2OH·HCl/NaOH) titration method described by Zhao and Heindel.[50]

Synthesis of CG-S-DOX prodrugs

CG-S-DOX prodrugs were synthesized via a Schiff base reaction between the CHO group of OCG and the amino group of DOX, according to the methodology described by Xu *et al.*[51] with some modifications. In detail, 10 mg of OCG (1.05×10^{-5} mol CHO) were dissolved overnight in 5 mL of DMSO at 70 °C in a round-bottomed flask. After complete dissolution, the flask was placed in a glycerin bath at 50 °C. In separate experiments, DOX·HCl was dissolved in DMSO, and triethylamine was added to remove hydrochloric acid (5 mol of trimethylamine to 1 mol of DOX·HCl). Subsequently, 6 mg of DOX (1.05×10^{-5} mol) was added to the flask and stirred for 72 h at 50 °C, in the dark. DMSO was removed by dialysis against distilled water using cellulose membranes (molecular weight cut-off 14 kDa) and monitored to determine the end of dialysis (3 days) using visible ultraviolet spectrophotometry (λ = 190-300 nm) and a Shimadzu® UV-1800 spectrophotometer (Japan). The resulting dispersion was freeze-dried and the prodrug was collected as a red solid.

The CG-A-DOX (cashew gum-amine bond-doxorubicin) prodrug was synthesized in a similar manner; however, after 72 h of reaction, $NaBH_4$ was used at a ratio molar 1:5 (mol CHO:mol $NaBH_4$) to reduce the imine bond (C=N) to an amine bond (C–N). In practice, 2 mg of $NaBH_4$ dissolved in distilled water (5 mL) were added to the reaction mixture, which was further stirred for 24 h at 50 °C, and then dialyzed against distilled water and freeze-dried.

Drug-binding capacity (DBC) and efficiency (DBE)

The amount of DOX linked to the prodrugs was determined using ultraviolet-visible (UV-Vis) spectrophotometry (λ_{abs} = 480 nm; Shimadzu UV-1800, Japan) and quantified using the calibration curve of DOX in DMSO (coefficient of determination (R^2) = 0.999). Briefly,

1 mg of the prodrug was dissolved in 3 mL of DMSO, and the absorbance at 480 nm was measured. DBC and DBE were calculated using equations 1 and 2,[52] respectively.

$$\mathrm{DBC}(\%) = \frac{\text{Mass of drug in prodrug}}{\text{Mass of prodrug}} \times 100 \quad (1)$$

$$\mathrm{DBE}(\%) = \frac{\text{Mass of drug in prodrug}}{\text{Total mass of feeding drug}} \times 100 \quad (2)$$

Preparation of prodrug nanoparticles

The prodrug nanoparticles were obtained via direct ultrasonication. One milligram of the prodrug was dissolved in 5 mL phosphate buffer (pH = 7.4, 0.1 mol L^{-1}) or distilled water and subjected to probe-type ultrasonic treatment (20 W, 6 cycles with 10 s active and 10 s off).

Fourier transform infrared (FTIR) spectroscopy

CG, OCG, and the prodrugs were mixed with potassium bromide (KBr) pellets and analyzed using a Shimadzu IR-Trace 100 spectrophotometer (Japan) in the region between 4000 and 400 cm^{-1}.

Proton nuclear magnetic resonance (^{1}H NMR)

CG, OCG, and the prodrugs were characterized using ^{1}H NMR spectroscopy. The analyses were performed at 30 °C on a Bruker advance model DRX500 (Germany) using DMSO-d_6 as the solvent, and the spectra were adjusted from the solvent signal.

High-performance liquid chromatography (HPLC)

HPLC analyses of DOX·HCl, CG-S-DOX and CG-A-DOX prodrug were performed using a Shimadzu liquid chromatography instrument (Japan) equipped with a model LC-10 AD pump, an SPD-M20A UV-Vis photodiode-array detector with a CBM-10 AD interface and a C18 column (10 µm, 15 cm × 4.6 mm) at 25 °C. The mobile phase consisted of 30% (v/v) of organic phase (acetonitrile) and 70% (v/v) of aqueous phase 30 mmol L^{-1} KH_2PO_4, 1% (v/v) trifluoroacetic acid) and a flow rate of 1.0 mL min^{-1}.

Size exclusion chromatography (SEC)

CG, OCG, and the prodrugs were characterized via SEC (Figure S1 and Table S1, Supplementary Information section) in a Shimadzu LC-20AD pump coupled to a refractive index detector (RID-10A) and using a linear PolySep-SEC GFC-P column (300 × 7.8 mm). The eluent was Milli-Q water containing $NaNO_3$ (0.1 mol L^{-1}) at a flow rate of 1.0 mL min^{-1} at 30 °C. The injection volume for each sample was 50 µL.

Critical aggregation concentration (CAC)

The prodrug CACs were determined via fluorescence spectroscopy using pyrene as the fluorescent probe on a fluorescence spectrometer (RF-6000 Shimadzu, Japan). Polarity influences vibronic band intensity in pyrene fluorescence and these perturbations can be used to accurately determine CAC in micellar systems.[53]

Experimentally, 5 mg of prodrug was dissolved in 25 mL of phosphate buffer (pH = 7.4, 0.1 mol L^{-1}) and subjected to probe-type ultrasonic treatment (20 W, 6 cycles with 10 s active and 10 s off). In a separate experiment, 40 µL pyrene solution in acetone (5.0×10^{-5} mol L^{-1}) were added to glass vials and acetone evaporated in a nitrogen atmosphere. Subsequently, the prodrug dissolved in the phosphate buffer was diluted to various concentrations and added to glass vials with pyrene at a pyrene concentration of 5×10^{-7} mol L^{-1}. The resultant dispersions were maintained overnight at room temperature (25 °C) to achieve equilibrium solubilization of pyrene in the hydrophobic domains of the self-assembled prodrugs. Then, the pyrene fluorescence emission spectrum (λ = 350-500 nm) was measured by setting the excitation wavelength (λ_{ex}) at 334 nm. The intensity ratio (I_{372}/I_{383}) *versus* prodrug concentration was used to determine CAC. The pyrene fluorescence excitation spectrum (λ = 320-350 nm) was obtained by setting the emission wavelength (λ_{em}) at 374 nm. The intensity ratio (I_{338}/I_{334}) *versus* prodrug concentration was used to determine CAC.

Dynamic light scattering (DLS)

The hydrodynamic diameter, polydispersity index (PDI), and zeta potential of the prodrug nanoparticles were determined using DLS on a Malvern ZS 3600 Nano Zetasizer equipment (United Kingdom). The hydrodynamic diameter and PDI were measured at 633 nm and a fixed propagation angle of 173° in phosphate buffer (pH = 7.4, 0.1 mol L^{-1}) at 37 °C and concentration of 200 µg mL^{-1}. The zeta potentials of the prodrug nanoparticles were measured at 25 °C in distilled water and concentration of 200 µg mL^{-1}. The samples were dispersed in distilled water or phosphate-buffered saline (PBS) and subjected to probe-type ultrasonic treatment (20 W, six cycles with 10 s active and 10 s off). Each measurement was performed in triplicate and without filtration.

Atomic force microscopy (AFM)

The prodrug nanoparticles were analyzed via AFM using an Asylum MFP-3D-Bio microscope (United Kingdom). The images were obtained in the intermittent contact mode (tapping mode), using microcantilevers (240AC-NA) with a nominal spring constant of 2 N m^{-1} and an amplitude frequency of 70 kHz. The samples were dispersed in distilled water (200 μg mL^{-1}), subjected to probe-type ultrasonic treatment (20 W, 6 cycles with 10 s active and 10 s off), and diluted to 1:200 (v/v). Subsequently, a 10 μL aliquot was removed and deposited on a mica surface, vacuum dried, and analyzed.

Scanning electron microscopy

The CG-S-DOX and CG-A-DOX prodrug nanoparticles were analyzed via SEM using a scanning electron microscope (SEM; Quanta 450 FEG; FEI, USA) at 30 kV. The prodrug dispersions were fixed in stubs with carbon tape, dried at room temperature (25 °C), and metallized with gold (QuorumQT150ES).

In vitro DOX release

The pH-responsive release of DOX, CG-S-DOX and CG-A-DOX prodrugs was evaluated in acetate (0.1 mol L^{-1}, pH = 5.0) and phosphate buffers (0.1 mol L^{-1}, pH = 7.4) at 37 °C, using the dialysis method. In brief, 1 mg of prodrug was dispersed in 5 mL of acetate or phosphate buffer using ultrasonic treatment (20 W, six cycles with 10 s active and 10 s off), and transferred to a cellulose membrane (molecular weight cut-off 1 kDa); next, it was placed in 50 mL of acetate or phosphate buffer with constant shaking (75 rpm) at 37 °C. Periodically, 3 mL of the released medium were collected and immediately replaced with an equal volume of fresh buffer. The amount of released DOX was determined using fluorescence spectroscopy (λ_{ex} = 480 nm and λ_{em} = 590 nm). The amount of released DOX was then converted to percentage of drug released according to the equation 3.

$$\text{Percentage of drug released}\,(\%) = \frac{M_t}{M_0} \times 100 \qquad (3)$$

where M_t is the amount of drug released at time t and M_0 is the initial amount of drug in the prodrug.

Cytotoxicity assay

Cytotoxicity was determined using the (3-[4,5-dimethylthiazol-2-yl]-2,5 diphenyl tetrazolium bromide) (MTT) assay.[54] HCT-116 (6×10^4 cell mL^{-1}), MCF-7 (1×10^5 cell mL^{-1}), and L929 (1×10^5 cell mL^{-1}) cells were seeded in 96-well plates. After 24 h of growth, the cells were treated with CG-S-DOX at concentrations ranging from 0.48 to 250 μg mL^{-1} (equivalent to 0.2-70 μg mL^{-1} of DOX) or CG-A-DOX at concentrations ranging from 7.8 to 250 μg mL^{-1} (equivalent to 1.8-60 μg mL^{-1} of DOX). OCG was tested at concentrations ranging from 7.8 to 250 μg mL^{-1}. DOX was used as positive control. The cells were incubated at 37 °C for 69 h. MTT solution was added to each well (0.5 mg mL^{-1}) and incubated for 3 h (total time 72 h). This reaction results in the reduction of MTT salt by cellular nicotinamide adenine dinucleotide phosphate (NADPH)-dependent oxidoreductase enzymes.[55] The MTT-formazan product dissolved in DMSO was estimated by measuring the absorbance at 595 nm using a multiwall microplate reader (Spectramax 190; Molecular Devices). Half maximal inhibitory concentration (IC_{50}) values with 95% confidence intervals ($CI_{95\%}$) were obtained by non-linear regression using the GraphPad Prism software.[56]

Cellular uptake assay

The cellular uptake of free DOX and CG-S-DOX prodrug nanoparticles was qualitatively investigated in HCT-116 cells using confocal laser scanning microscopy (CLSM; LSM 710; Zeiss, Germany). HCT-116 cells were seeded in 12-well plates (5×10^4 cells $well^{-1}$) in Dulbecco's modified eagle medium (DMEM) with 10% fetal bovine serum (FBS) and 1% penicillin (100 U mL^{-1}) and streptomycin (100 μg mL^{-1}) over a sterile cover slip. The cells were incubated at 37 °C with free DOX (0.12 μg mL^{-1}) or CG-S-DOX prodrug nanoparticles (4.7 μg mL^{-1}, equivalent to 1.3 μg mL^{-1} of DOX) for 24 h. After incubation, the cells were washed with PBS, fixed with 4% (m/v) PBS-buffered paraformaldehyde and the cellular nuclei were stained with 4',6-diamidino-2-phenylindole (DAPI). The excitation wavelengths were 405 and 488 nm and the emission wavelength ranges were 425-475 and 500-580 nm for DAPI (blue) and DOX (red), respectively.

Statistical analysis

All experiments were carried out in triplicate and the data were obtained as the mean ± standard deviation (S.D.). Statistical analysis was performed using one-way analysis of variance (ANOVA) followed by Tukey's test ($p < 0.05$) or two-way ANOVA followed by Dunnett's test ($p < 0.05$), using OriginPro 8.5[57] or the GraphPad Prism software.[56]

Results and Discussion

Synthesis and characterization

The synthesis of CG-S-DOX and CG-A-DOX prodrugs is illustrated in Scheme 1. First, OCG was obtained by oxidizing CG vicinal OH groups to CHO groups using $NaOI_4$ (Scheme 1a). The CHO content in OCG was quantified as 1.05 mmol g^{-1} (8.5% oxidized units). Subsequently, CG-S-DOX and CG-A-DOX prodrugs were synthesized via a Schiff base reaction between the CHO group of OCG and the amino group of DOX (Scheme 1b), without and with imine reduction, respectively.

The chemical structures of CG, OCG, DOX·HCl, and prodrugs were analyzed using FTIR (Figure 1). The FTIR spectra of CG and OCG (Figure 1a) showed similar bands at 3700-3000 cm^{-1}, attributed to OH stretching vibrations; at 2930 and 2893 cm^{-1}, corresponding to the symmetric and asymmetric CH stretching vibration; the broad band at 1640 cm^{-1}, related to the asymmetric stretching vibration of the carboxylate group (COO^-) and also to OH scissor vibrations of bonded water molecules; band at 1415 cm^{-1}, correspond to the symmetric stretching vibration of the carboxylate group (COO^-); and the bands at 1150, 1080, and 1030 cm^{-1} are characteristic of the COC stretching vibration of the glycosidic bonds and OH deformation of alcohols. Spectral differences were observed at 1735 cm^{-1} with the appearance of a new band corresponding to the C=O stretching vibration of the CHO group in the OCG spectrum.[30,31]

The FTIR spectrum of DOX (Figure 1b) showed multiple bands at 3525 cm^{-1}, attributed to the N–H

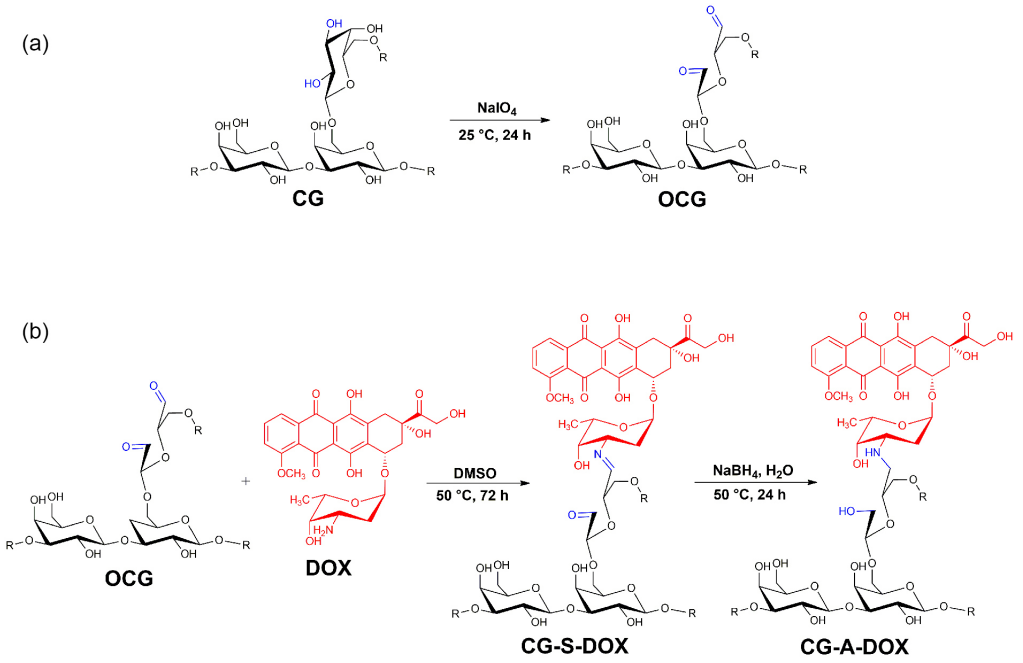

Scheme 1. Schematic illustration for the oxidation of CG (a) and synthesis of CG-DOX prodrugs (b).

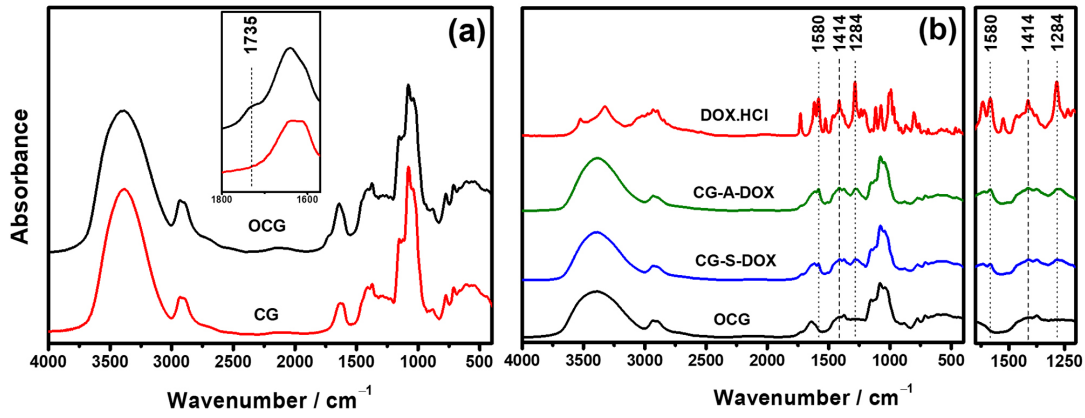

Figure 1. FTIR (KBr) spectra of CG and OCG samples (a) and DOX·HCl, CG-S-DOX, and CG-A-DOX (b).

symmetric stretching vibration; at 3325 cm^{-1} due to the OH stretching vibration; 3100-2800 cm^{-1}, corresponding to the CH stretching vibration; 1730 and 1615 cm^{-1} owing to the C=O stretching vibration of ketone and quinone; and at 1116, 1072, and 1006 cm^{-1}, corresponding to the OH stretching vibration of tertiary, secondary, and primary alcohols, respectively.[58,59] Three new peaks were observed in the CG-S-DOX and CG-A-DOX spectra (Figure 1b) compared to the OCG spectrum (Figure 1a): at 1580 cm^{-1}, attributed to the C=C stretching vibration of the aromatic ring; at 1414 cm^{-1}, related to the CH symmetric bending vibration of the methyl group (CH_3); and at 1284 cm^{-1}, corresponding to the COC stretching vibration of DOX. These results suggest conjugation of the drug with the polysaccharide.[12,60] The absorption bands corresponding to the Schiff base bond (C=N, 1690-1640 cm^{-1}) and amine bond (C–N, 1230-1030 cm^{-1}) could not be detected, as they may be overlapped with polysaccharide bands.

The conjugation between the CHO group of OCG and the amine group of DOX was confirmed using ^{1}H NMR spectroscopy (Figure 2). As reported by Maciel *et al.*[30] the anomeric protons of CG can be observed at 4.95 ppm (α-D-glucose), 4.81 ppm (α-L-rhamnose), 4.69 and 4.44 ppm (β-D-galactose 1→3), 4.50 ppm (β-D-glucuronic acid), and 4.39 ppm (β-D-galactose 1→6), with 1.3 ppm denoting the peak of the CH_3 of rhamnose. Comparing the CG and OCG spectra, new peaks can be observed in the region 7.30-9.30 ppm that can be attributed to the free CHOs of the different monosaccharide units of OCG, confirming the introduction of CHO groups in the CG structure. Similar results were obtained by Maciel *et al.*[30] for oxidized CG derivatives. The disappearance of the characteristic peaks of the free CHOs of the different OCG monosaccharide units (7.30-9.30 ppm) and the appearance of new peaks corresponding to the aromatic protons of DOX (7.5-8.0 ppm) confirmed the formation of CG-S-DOX and CG-A-DOX prodrugs.[59]

The HPLC chromatograms (Figure 3) confirm that the amino group of the DOX has been conjugated onto the aldehyde group of the OCG. The different retention times for free DOX (5.56 min) compared to CG-S-DOX (4.87 min) and CG-A-DOX (4.93 min) prodrugs indicate that the structure of DOX has been changed.[61] In other words, DOX is covalently linked to CG polysaccharide.

The reaction efficiencies, obtained by estimating DBC and DBE, were determined via UV-Vis spectrophotometry using the standard curve method, and the results are listed in Table 1. The DBE values for CG-S-DOX (75%) and CG-A-DOX (64%) prodrugs are higher than those for the dextran-DOX prodrugs (19.2 and 24%)[52] and starch-DOX prodrug (59%)[62] under the same synthesis conditions (1 mol of

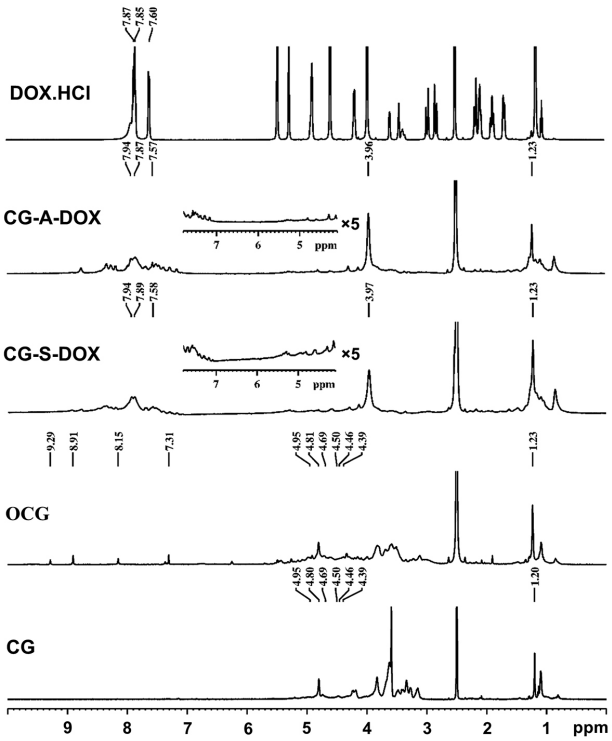

Figure 2. ^{1}H NMR spectra (500 MHz, DMSO-d_6) of CG, OCG, CG-S-DOX, CG-A-DOX, and DOX·HCl in DMSO-d_6 at 30 ºC.

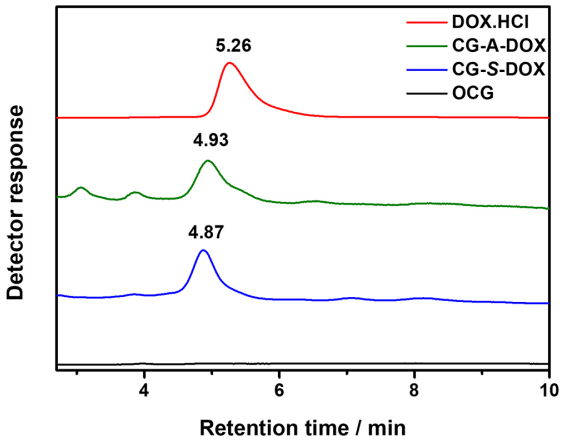

Figure 3. HPLC chromatograms of OCG, DOX·HCl, CG-S-DOX and CG-A-DOX prodrug using 30% of acetonitrile and 70% of KH_2PO_4 (30 mM, 1% (v/v) trifluoroacetic acid) as the eluent with a flow rate of 1.0 mL min^{-1}.

CHO:1 mol DOX, 72 h of reaction at 50 °C). In addition, the DBE values of the CG-S-DOX and CG-A-DOX prodrugs were higher than those of the hyaluronic acid-DOX prodrug (26%)[63] synthesized at 25 °C and dextran-DOX prodrug (45.7%)[18] synthesized at 60 °C using Schiff base reaction. These results confirm that the synthesis conditions used in the present study were better optimized than those reported in the literature.

CAC is an important parameter for demonstrating the self-assembly capabilities of amphiphilic materials. The

Table 1. Properties of the prodrugs

Prodrug	Yield / %	DBC / %	DBE / %	CAC / (μg mL^{-1})
CG-S-DOX	81 ± 1^{a}	28 ± 1^{a}	75 ± 1^{a}	27 ± 1^{a}
CG-A-DOX	80 ± 1^{a}	24 ± 1^{b}	64 ± 2^{b}	32 ± 2^{b}

Data are presented as the mean ± S.D. (n = 3). Statistical analysis was performed using one-way ANOVA, followed by Tukey's test. Means with the same superscript letters in a column are not significantly different ($p > 0.05$), whereas those with different letters in the same column are ($p < 0.05$). DBC: drug-binding capacity; DBE: drug-binding efficiency; CAC: critical aggregation concentration.

CG-S-DOX and CG-A-DOX prodrugs can self-assemble in water into a core-shell structure, in which DOX and CG constitute the hydrophobic core and hydrophilic shell, respectively. Figures 4a and 4b show the pyrene fluorescence intensity ratio (I_{372}/I_{383} and I_{338}/I_{334}) as a function of the concentration of the prodrugs, where I_{372}/I_{383} and I_{338}/I_{334} remained constant up to the concentration limit.

The concentration limit reflects prodrug CAC; that is, the minimum concentration required to form a micellar system. The CAC values were obtained from the crossover point between the lines in Figure 4 and are listed in Table 1. The CAC values obtained for the CG-S-DOX (27 μg mL^{-1}) and CG-A-DOX (32 μg mL^{-1}) prodrugs were lower than those reported by Niu *et al.*[60] for a dextran-DOX prodrug (CAC = 66 μg mL^{-1} and DBC = 22.5%). The CAC values of the CG-S-DOX and CG-A-DOX prodrugs were inversely proportional to the DBC values, likely because, with increasing DBC, an increase in prodrug hydrophobicity reduces the concentration of prodrug necessary for the formation of nanoparticles. Similar behavior was observed by Curcio *et al.*[64] for DOX-dextran-lipoic acid prodrugs.

Size distribution and morphological analysis

The prodrug nanoparticle dispersions were obtained using the direct ultrasound method and characterized using DLS, SEM, and AFM (Table 2). The prodrug nanoparticles characterized via DLS showed unimodal size distributions (Figures 4c and 4d) in phosphate buffer (pH = 7.4, 0.1 mol L^{-1}). The obtained average sizes were 159 nm (CG-S-DOX) and 193 nm (CG-A-DOX) and the PDI values were lower than 0.3, indicating good homogeneity of the prodrug nanoparticles and negative zeta potentials in water.

The average size differences between the CG-S-DOX (159 nm) and CG-A-DOX (193 nm) prodrugs are associated with the high DBC value of CG-S-DOX (Table 1), because the increase in DBC hydrophobicity of the CG-S-DOX prodrug reduces the average nanoparticle size due to

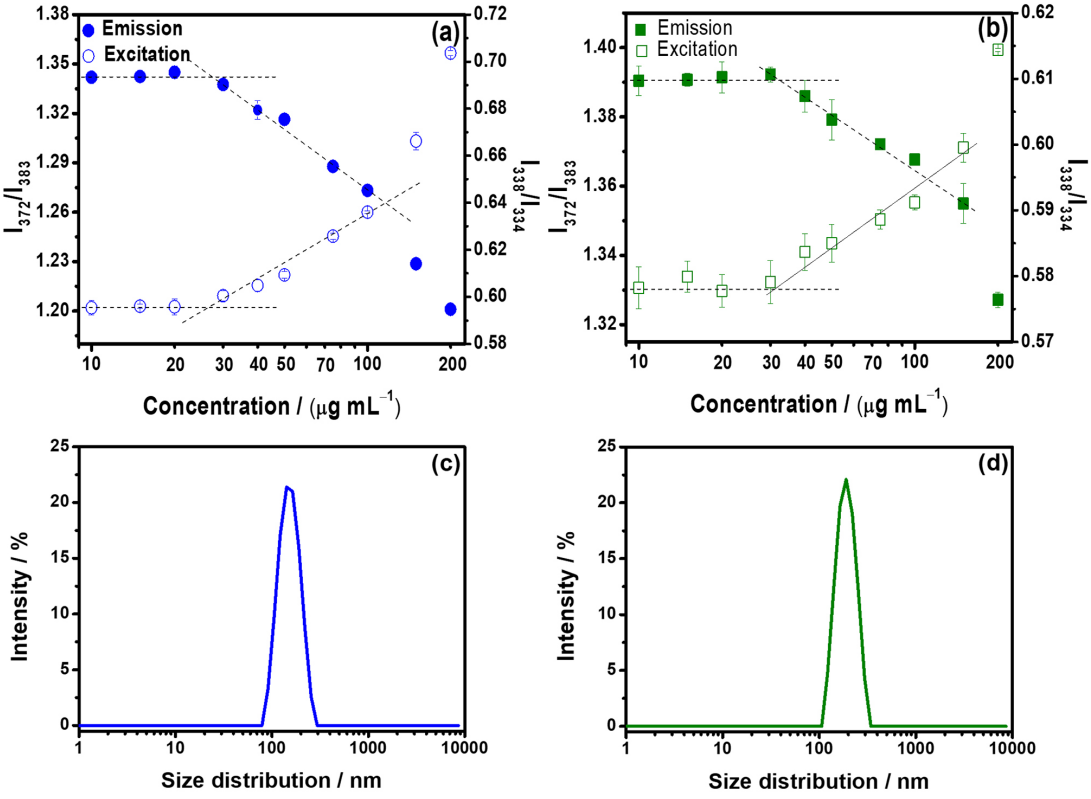

Figure 4. Dependence of the pyrene fluorescence intensity ratio (I_{372}/I_{383} and I_{338}/I_{334}) versus the concentration of CG-S-DOX (a) and CG-A-DOX (b) in phosphate buffer (pH = 7.4 at 37 °C). Size distribution of CG-S-DOX (c) and CG-A-DOX (d) nanoparticles in phosphate buffer (pH = 7.4 at 37 °C).

Table 2. Physicochemical parameters of the prodrug nanoparticles

Sample	DLS			SEM	AFM
	Size[A] / nm	PDI	Zeta potential[B] / mV	Size / nm	Size / nm
CG-S-DOX	159 ± 11[a]	0.29 ± 0.06[a]	–18 ± 2[a]	74 ± 16[a]	ca. 20
CG-A-DOX	193 ± 8[b]	0.28 ± 0.03[a]	–20 ± 2[a]	75 ± 10[a]	ca. 62

Data are presented as the mean ± S.D. (n = 3). Statistical analysis was performed using one-way ANOVA, followed by Tukey's test. Means with the same letters in a column are not significantly different ($p > 0.05$), while those with different letters are ($p < 0.05$). [A]Phosphate buffer (pH = 7.4, 0.1 mol L^{-1}) at 37 °C; [B]water at 25 °C. DLS: dynamic light scattering; SEM: scanning electron microscope; AFM: atomic force microscopy; PDI: polydispersity index.

increased hydrophobic interactions. Nanoparticles smaller than 200 nm are ideal for intravenous applications against cancer cells owing to passive targeting via the EPR effect.[65] The CG-S-DOX and CG-A-DOX prodrug nanoparticles have excellent sizes for intravenous application and for promoting DOX accumulation inside tumors through passive targeting via the EPR effect.

AFM and SEM analyses showed that the prodrug nanoparticles had a spherical shape and smooth surface (Figure 5). The differences in average size using DLS, SEM, and AFM (Table 2) are because AFM and SEM analyses allow determination of the size of the dry nanoparticles, whereas DLS measures the hydrodynamic diameter of the nanoparticles in solution; this includes the ionic layers and solvents associated with the nanoparticles.[66] Similar behavior was observed for prodrug nanoparticles by Li *et al.*[62] who reported sizes in the range of 25-31 nm, determined using transmission electron microscopy, and 52-73 nm using DLS.

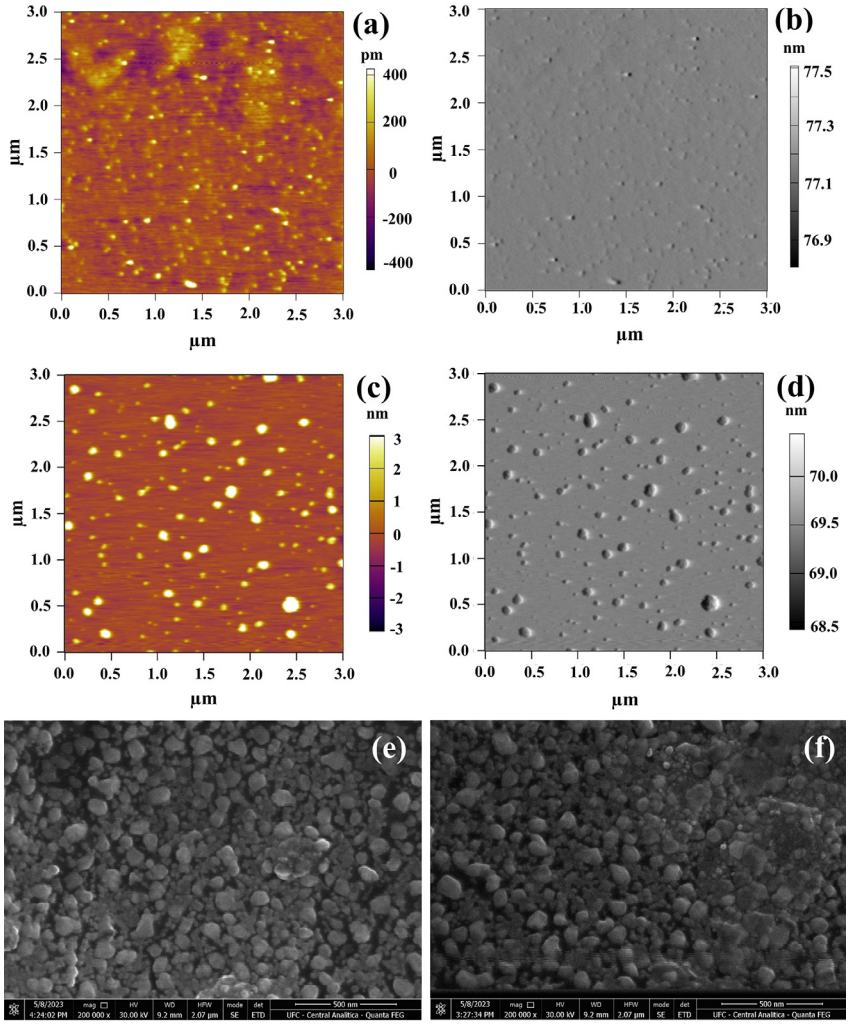

Figure 5. AFM images of CG-S-DOX prodrug nanoparticles (a and b) and CG-A-DOX prodrug nanoparticles (c and d). (a) and (c), height images. (b) and (d), amplified images. SEM images of CG-S-DOX (e) and CG-A-DOX (f).

In vitro DOX release and cytotoxicity assay

An initial burst release of DOX was observed for both matrices during the first hour of the release experiment, owing to non-linked DOX encapsulated in the self-assembly process of the prodrug nanoparticle formation. The influence of pH on the rate of DOX release from the CG-S-DOX and CG-A-DOX prodrug nanoparticles is shown in Figure 6.

The release-rate profiles were more differentiated for CG-S-DOX in the pH values investigated (5.0 and 7.4) than for CG-A-DOX. A steady plateau was reached after a 24 h release time for both prodrugs. After 72 h, 30 and 32% of DOX was released from CG-S-DOX and CG-A-DOX prodrug nanoparticles, respectively, at pH 7.4 (normal tissue), while, at pH 5.0 (intracellular tumor microenvironment), the percentages were 54 and 40%, respectively.

The pH had a greater influence on DOX release rate from the CG-S-DOX prodrug nanoparticles than from the CG-A-DOX prodrug nanoparticles. This is because the imine/Schiff base bond (C=N) is more susceptible to cleavage in acidic environments than the amine bond (C–N). Similar behavior was observed by Xu *et al.*[51] for the DOX release rate from dextran-DOX prodrug nanoparticles. Dextran-graft-poly (*N*-isopropylacrylamide)/DOX (pH 7.4: 35% and pH 5.0: 59%),[11] dextran-DOX (pH 7.4: 32% and pH 5.0: 57%)[60] and starch-DOX (pH 7.4: 38% and pH 5.5: 60%)[67] prodrug nanoparticles synthesized via Schiff base showed DOX release rates similar to that for CG-S-DOX. These results suggest that the generated prodrug nanoparticles have a pH-responsive and controlled release profile that promotes DOX controlled release in the tumor microenvironment.

The kinetic mechanism by which a burst occurs, followed by a steady release, can be described by the model proposed by Zeng *et al.*[68] (equation 4):

$$\frac{M_t}{M_0} = \frac{k_{off}}{k_{on} + k_{off}}\left(1 - e^{k_s t}\right) + \frac{k_{on}}{k_{on} + k_{off}}\left(1 - e^{k_{off} t}\right) \quad (4)$$

where k_s is the diffusion rate, k_{on} is the drug association rate constant, and k_{off} is the drug dissociation rate constant. The model assumes that $k_s >> k_{on}$ and $k_s >> k_{off}$. This model had a good fit with R^2 values higher than 0.98.

The bound state of a drug in a matrix can be evaluated using the free energy (ΔG) associated with the delivery system (equation 5).

$$\Delta G = -k_B T \ln\left(k_{on} / k_{off}\right) \quad (5)$$

where k_B is Boltzmann's constant and T is the absolute temperature (310 K).

The model parameters for the prodrug systems at two different pH values are shown in Table 3. For CG-S-DOX, greater ΔG values at pH 5.0 than at pH 7.4 were observed, which confirms the reduced interaction of the drug with the matrix at pH 5.0, owing to the susceptibility of the Schiff base at this pH environment. Compared with the prodrug obtained by reducing the imide bond (CG-A-DOX), at both investigated pH values, ΔG values were lower in relation to the prodrug CG-S-DOX, indicating greater interaction between DOX and CG and, consequently, decreased DOX release.

The cytotoxicity of the free DOX, OCG, and CG-S-DOX and CG-A-DOX prodrugs was evaluated in L929 (murine fibroblast non-tumor), HCT-116 (human colorectal cancer), and MCF-7 (human breast cancer) cells using MTT assays after 72 h of incubation (Figure 7 and Table 4). OCG did not show cytotoxicity against non-tumor cells (L929) at concentrations of up to 250 μg mL^{-1}.

The CG-S-DOX prodrug nanoparticles showed significantly decreased cytotoxicity against non-tumor cells (L929) compared to free DOX. The IC_{50} (for various DOX concentrations) of CG-S-DOX was

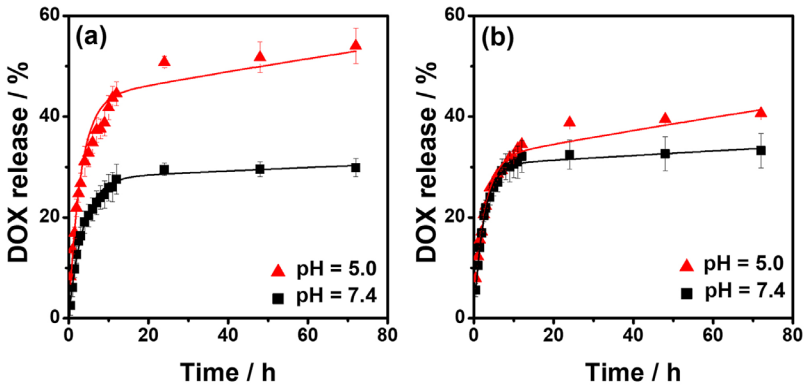

Figure 6. pH-dependent DOX release profiles from the CG–S–DOX (a) and CG-A-DOX; (b) nanoparticles.

Table 3. Second order exponential order parameters for the CG-S-DOX and CG-A-DOX prodrug nanoparticles

Nanoparticle	pH	Model parameter				
		k_s / h^{-1}	k_{on} / 10^{-3} h^{-1}	k_{off} / h^{-1}	ΔG / 10^{-21} J	R^2
CG-S-DOX	5.0	0.34	3.39	2.59×10^{-3}	−1.15	0.980
	7.4	0.28	1.29	4.96×10^{-4}	−4.09	0.990
CG-A-DOX	5.0	0.38	4.58	2.12×10^{-3}	−3.29	0.984
	7.4	0.41	1.56	6.80×10^{-4}	−9.82	0.996

k_s: the diffusion rate constant; k_{on}: the drug association rate constant; k_{off}: the drug dissociation rate constant; ΔG: Gibbs free energy; R^2: coefficient of determination.

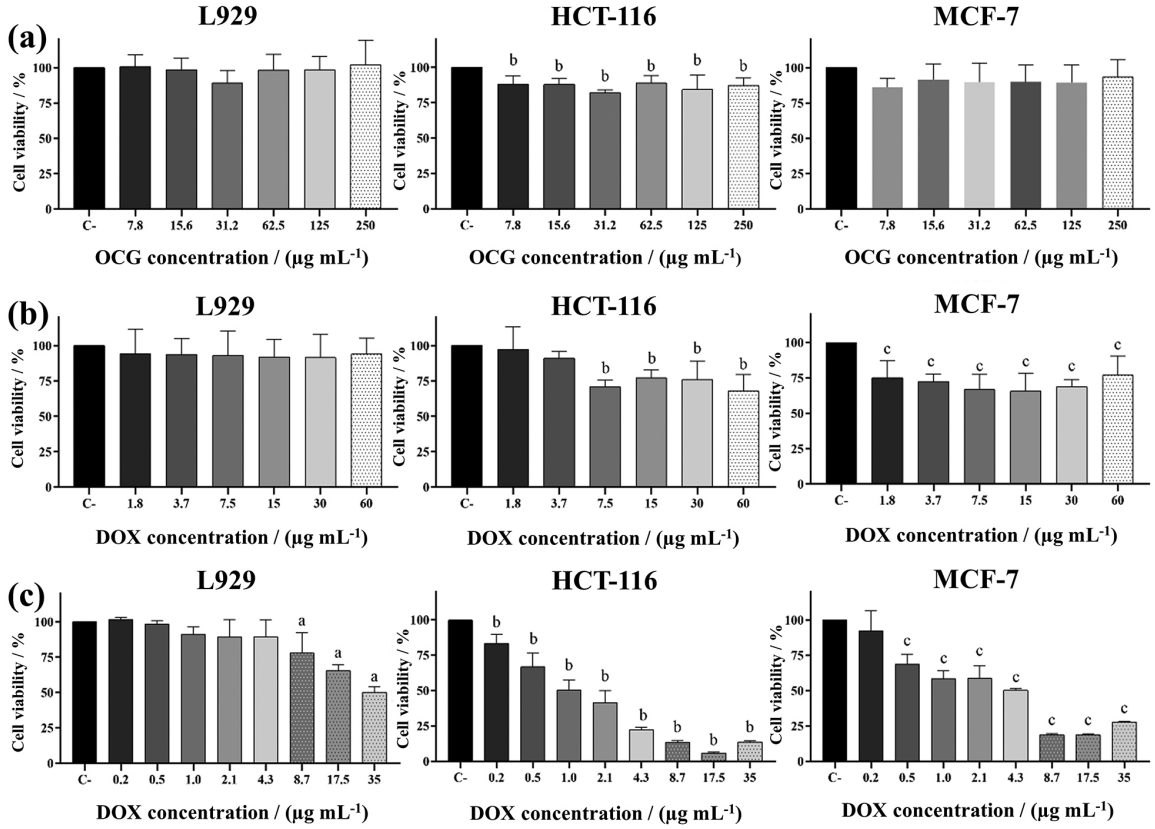

Figure 7. Cytotoxicity of OCG (a), CG-A-DOX (b), and CG-S-DOX (c) against tumor and non-tumor cell lines. Cell viability values obtained using MTT assays after 72 h of incubation. Data are presented as the mean ± S.D. from at least two independent experiments performed in triplicate. Dulbecco's Modified Eagle Medium (DMEM) was used as a negative control (C–). $p < 0.05$ compared to negative control of (a) L929 cells, (b) HCT-116 cells and (c) MCF-7 cells using ANOVA, followed by Dunnett's test.

Table 4. Evaluation of *in vitro* cytotoxic activity in L929, HCT-116, and MCF-7 cells

Sample	IC_{50} (SI) / (μg mL^{-1})		
	L929	HCT-116	MCF-7
CG-S-DOX[a]	28.20 ± 4.40	1.33 ± 0.25 (21.2)	2.86 ± 1.08 (9.86)
CG-A-DOX[a]	> 120	> 60	> 60
OCG	> 250	> 250	> 250
DOX	0.42 ± 0.16	0.12 ± 0.03 (3.5)	0.29 ± 0.08 (1.45)

IC_{50} values were obtained using the MTT method after 72 h of incubation. Data are presented as IC_{50} values and 95% confidence intervals. [a]DOX concentration. DOX: doxorubicin; SI: selectivity index (data in parentheses).

67 times higher (IC_{50} = 28.2 μg mL^{-1}) than that of free DOX (IC_{50} = 0.42 μg mL^{-1}). Similar behavior has been observed for alginate-DOX prodrug nanoparticles (IC_{50} = 192.3 μg mL^{-1}/IC_{50} = 1.7 μg mL^{-1}) tested against MCF-10A cells (human breast epithelial cell line).[12] The CG-A-DOX prodrug nanoparticles did not present cytotoxicity against any of the tested tumor cells at a prodrug concentration of 250 μg mL^{-1} (equivalent to 60 μg mL^{-1} of DOX), because DOX is strongly bound to CG via amine bonding, which is not pH sensitive and leads to decreased DOX release.

In contrast, CG-S-DOX prodrug nanoparticles exhibited

cytotoxicity against all tested tumor cells, with IC_{50} values ranging between 1.31 and 2.74 μg mL^{-1} in HCT-116 and MCF-7 cells, respectively. The CG-S-DOX prodrug nanoparticles showed IC_{50} values that were 11 and 9.4 times higher (in DOX concentration) than those of the free DOX (Table 4), which may be related to slow release kinetics (Figure 6a) and slow internalization in cells.[69] Similar behavior has been reported for dextran-DOX prodrug nanoparticles.[10,60] However, the IC_{50} of CG-S-DOX prodrug nanoparticles (IC_{50} = 2.74 μg mL^{-1}) was lower than that of alginate-DOX prodrug (IC_{50} = 6.70 μg mL^{-1})[14] and polyester-based nanoparticles for DOX and curcumin co-delivery (IC_{50} = 11.46 μg mL^{-1})[70] against MCF-7 cells and dextran-graft-poly (*N*-isopropylacrylamide)/DOX nanoparticles (IC_{50} = 9.03 μg mL^{-1})[11] against HCT-116 cells. These data indicate that the CG-S-DOX prodrug nanoparticles have better anticancer activity than previously reported DOX prodrug delivery systems. In addition, the CG-S-DOX prodrug nanoparticles showed a controlled and pH-responsive release profile, have ideal sizes to promote DOX accumulation inside tumor cells via the EPR effect, and exhibit low toxicity.

The selectivity index (SI) is a measure of the drug's activity in tumor cell lines compared to its activity in normal cells. SI values can be calculated using the equation 6:

$$SI = \frac{L929\ IC_{50}}{Cancer\ cell\ IC_{50}} \quad (6)$$

Suffness and Pezzuto[71] proposed that SI values equal to or higher than 2 are considered significant, indicating that the compound has at least a two-fold higher activity against tumor cell lines compared to normal cells.

The SI values observed for CG-S-DOX in HCT-116 and MCF-7 are 6.1 and 6.8 times higher, respectively, than those observed for DOX. This higher selectivity for tumor cells compared to normal cells corroborates with our finds.

Cellular uptake assay

The intracellular internalization of free DOX and CG-S-DOX prodrug nanoparticles was studied qualitatively in HCT-116 cells. The results showed that free DOX and CG-S-DOX prodrug nanoparticles were taken up by tumor cells after 24 h of incubation and reached both the cytoplasm and nucleus (Figure 8). Free DOX mainly accumulated in

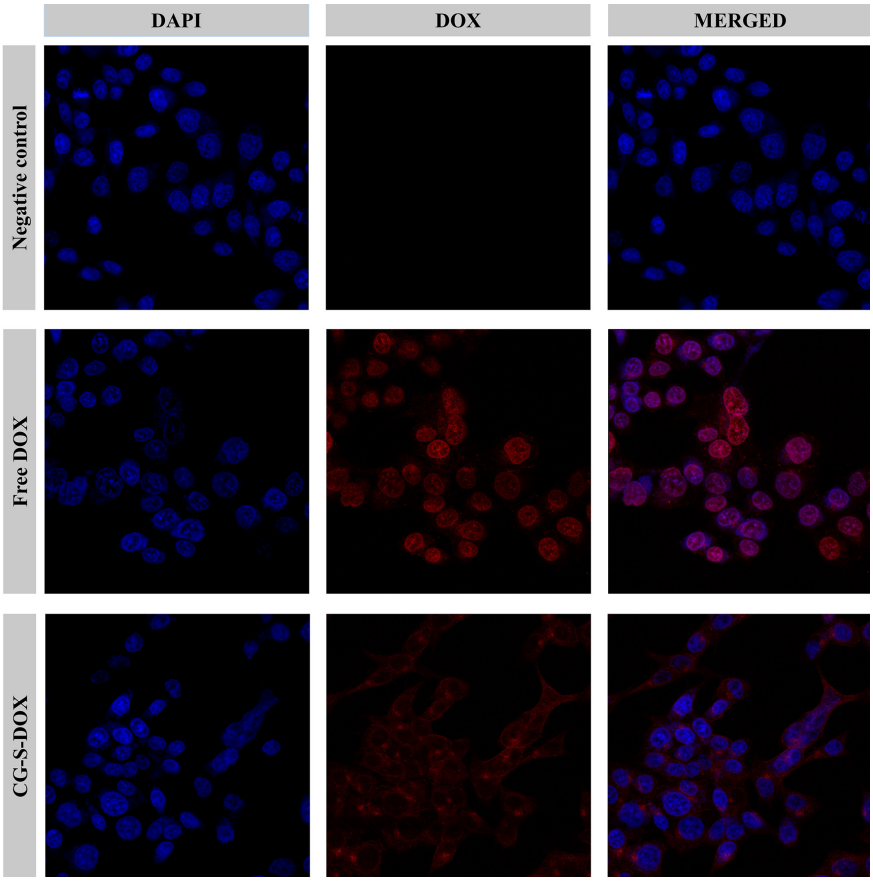

Figure 8. Uptake of free DOX and CG-S-DOX prodrug nanoparticles by HCT-116 cells after 24 h incubation was observed using CLSM. Cell nuclei were stained with DAPI (blue) and red fluorescence represents DOX.

the nucleus, whereas the CG-S-DOX prodrug nanoparticles were distributed in the cytoplasm and nucleus, with a higher concentration (red fluorescence) in the cytoplasm. This behavior can be attributed to different cellular uptake pathways, that is, the diffusion of free DOX and endocytosis of CG-S-DOX prodrug nanoparticles. Similar behavior was observed for dextran-graft-poly (*N*-isopropylacrylamide)/DOX nanoparticles in HCT-116 cells[11] and dextran-DOX prodrugs in SW1353 cells.[60] These results, together with our cytotoxicity analyses, confirm the potential of CG-S-DOX prodrug nanoparticles as a reliable and efficient system for the selective delivery of DOX in tumor cells.

Conclusions

Prodrugs were successfully synthesized via Schiff base (CG-S-DOX) or amine bond (CG-A-DOX) formation between the amino group of DOX and the CHO group of oxidized cashew gum. The prodrugs could self-assemble in water, forming nanoparticles with hydrodynamic diameters smaller than 200 nm and a zeta potential of approximately –20 mV, that are suitable for intravenous application. The nanoparticles produced via self-assembly exhibited a pH-responsive and controlled DOX-release profile. The drug-binding content and efficiency of the DOX-CG prodrug systems were higher than those of other polysaccharide-based prodrugs, resulting in lower critical aggregation concentrations. A significant decrease in cytotoxicity against non-tumor cells (L929) was observed for CG-A-DOX and CG-S-DOX prodrug nanoparticles compared to free DOX. CG-A-DOX exhibited low cytotoxicity against the tested tumor cell lines (HCT-116 and MCF-7), in contrast to the CG-S-DOX prodrug nanoparticles that showed intracellular internalization in tumor cells (HCT-116) and antitumor activity against HCT-116 and MCF-7 cells and lower IC_{50} values when compared with other polysaccharide-DOX conjugate systems. Therefore, the CG-S-DOX prodrug nanoparticles show great potential for promoting effective delivery of DOX to tumor cells.

Supplementary Information

Supplementary information (chromatograms of CG, OCG and prodrugs obtained by size exclusion chromatography (SEC) were reported in Figure S1, as well as molar mass data (Table S1)) is available free of charge at http://jbcs.sbq.org.br as PDF file.

Acknowledgments

This study was partially supported by Brazilian agencies MCTI/CNPq (grant No. 406973/2022-9) INCT/Polysaccharides (National Technology-Science Institute for Polysaccharides); INCTBioNat (CNPQ grant No. 465637/2014-0 and FAPESP grant No. 2014/50926-0, Brazil); Coordenação de Aperfeiçoamento de Pessoal de Nível Superior - Brazil (CAPES) - Finance Code 001 (PROEX 23038.000509/2020-82), FINEP (CV.01.22.0174.00), and CNPq (grant numbers: 408511/2016-8); and Fundação Cearense de Amparo à Pesquisa (MLC-0191-000153.01.00/22). The authors gratefully acknowledge CENAUREM for the NMR analyses and Central Analítica-UFC/CT-INFRA/MCTI-SISANO/Pró-Equipamentos CAPES for support.

Author Contributions

Irisvan S. Ribeiro was responsible for conceptualization, methodology, validation, formal analysis, investigation, writing original draft; Adisom L. S. Leornado, Maria J. M. Carneiro, Rosemayre S. Freire for performed the experiments; Jeanlex S. Sousa, José. D. B. Marinho Filho, Ana J. Araújo for methodology, investigation and visualization; Haroldo C. B. Paula for validation, data curation and writing review and editing; Raimundo N. Costa Filho for validation, data curation; Judith P. A. Feitosa for funding acquisition, writing review and editing, supervision; Regina C. M. de Paula for conceptualization, methodology, writing review and editing, supervision, resources, project administration and funding acquisition.

References

1. Ding, C.; Chen, C.; Zeng, X.; Chen, H.; Zhao, Y.; *ACS Nano* **2022**, *16*, 13513. [Crossref]
2. Zhao, B.; Chen, S.; Hong, Y.; Jia, L.; Zhou, Y.; He, X.; Wang, Y.; Tian, Z.; Yang, Z.; Gao, D.; *Pharmaceutics* **2022**, *14*, 1522. [Crossref]
3. Han, S.; Lee, J.; Jung, E.; Park, S.; Sagawa, A.; Shibasaki, Y.; Lee, D.; Kim, BS.; *ACS Appl. Bio Mater.* **2021**, *4*, 2465. [Crossref]
4. Kalva, N.; Uthaman, S.; Lee, S. J.; Lim, Y. J.; Augustine, R.; Huh, K. M.; Park, I. K.; Kim, I.; *React. Funct. Polym.* **2021**, *166*, 104966. [Crossref]
5. Luo, Q.; Lin, L.; Huang, Q.; Duan, Z.; Gu, L.; Zhang, H.; Gu, Z.; Gong, Q.; Luo, K.; *Acta Biomater.* **2022**, *143*, 320. [Crossref]
6. Carmona-Fontaine, C.; Bucci, V.; Akkari, L.; Deforet, M.; Joyce, J. A.; Xavier, J. B.; *Proc. Natl. Acad. Sci. U.S.A.* **2013**, *110*, 19402. [Crossref]
7. Zhao, K.; Li, D.; Xu, W.; Ding, J.; Jiang, W.; Li, M.; Wang, C.; Chen, X.; *Biomaterials* **2017**, *116*, 82. [Crossref]
8. Li, M.; Sun, J.; Zhang, W.; Zhao, Y.; Zhang, S.; Zhang, S.; *Carbohydr. Polym.* **2021**, *251*, 117103. [Crossref]

9. Wang, W.; Li, M.; Zhang, Z.; Cui, C.; Zhou, J.; Yin, L.; Lv, H.; *Carbohydr. Polym.* **2017**, *156*, 97. [Crossref]
10. Zhang, X.; Li, D.; Huang, J.; Ou, K.; Yan, B.; Shi, F.; Zhang, J.; Zhang, J.; Pang, J.; Kang, Y.; Wu, J.; *J. Mater. Chem. B* **2019**, *7*, 251. [Crossref]
11. Carneiro, M. J. M.; Paula, C. B. A.; Ribeiro, I. S.; Lima, L. R. M.; Ribeiro, F. O. S.; Silva, D. A.; Araújo, G. S.; Marinho Filho, J. D. B.; Araújo, A. J.; Freire, R. S.; Feitosa, J. P. A.; de Paula, R. C. M.; *Int. J. Biol. Macromol.* **2021**, *185*, 390. [Crossref]
12. Gao, C.; Tang, F.; Gong, G.; Zhang, J.; Hoi, M. P. M.; Lee, S. M. Y.; Wang, R.; *Nanoscale* **2017**, *9*, 12533. [Crossref]
13. Xiong, H.; Ni, J.; Jiang, Z.; Tian, F.; Zhou, J.; Yao, J.; *Biomater. Sci.* **2018**, *6*, 2527. [Crossref]
14. Mansur, A. A. P.; Carvalho, S. M.; Lobato, Z. I. P.; Leite, M. D. F.; Cunha, A. D. S.; Mansur, H. S.; *Bioconjugate Chem.* **2018**, *29*, 1973. [Crossref]
15. Zhang, Y. H.; Zhang, Y. M.; Yu, J.; Wang, J.; Liu, Y.; *Chem. Comm.* **2019**, *55*, 1164. [Crossref]
16. Duan, Y.; Li, K.; Wang, H.; Wu, T.; Zhao, Y.; Li, H.; Tang, H.; Yang, W.; *Carbohydr. Polym.* **2020**, *238*, 116195. [Crossref]
17. Yin, T.; Wang, Y.; Chu, X.; Fu, Y.; Wang, L.; Zhou, J.; Tang, X.; Liu, J.; Huo, M.; *ACS Appl. Mater. Interfaces* **2018**, *10*, 35693. [Crossref]
18. Li, D.; Su, T.; Ma, L.; Yin, F.; Xu, W.; Ding, J.; Li, Z.; *Eur. J. Med. Chem.* **2020**, *199*, 112367. [Crossref]
19. Pires, N. R.; Santos, C. M. W.; Sousa, R. R.; de Paula, R. C. M.; Cunha, P. L. R.; Feitosa, J. P. A. F.; *J. Braz. Chem. Soc.* **2015**, *26*, 1274. [Crossref]
20. Amorim, A. G. N.; Sánchez-Paniagua, M.; Oliveira, T. M.; Mafud, A. C.; Silva, D. A.; Leite, J. R. S. A.; López-Ruiz, B.; *J. Mater. Chem. B* **2021**, *9*, 6825. [Crossref]
21. Melo, A. M. A.; Oliveira, M. R. F.; Furtado, R. F.; Borges, M. F.; Biswas, A.; Cheng, H. N.; Alves, C. R.; *Carbohydr. Polym.* **2020**, *228*, 115408. [Crossref]
22. de Oliveira, W. Q.; Wurlitzer, N. J.; Araújo, A. W. O.; Comunian, T. A.; Bastos, M. S. R.; de Oliveira, A. L.; Magalhães, H. C. R.; Ribeiro, H. L.; de Figueiredo, R. W.; de Sousa, P. H. M.; *Food Res. Int.* **2020**, *131*, 109047. [Crossref]
23. Ferreira, S. R. S.; Mesquita, M. V. N.; Sá, L. L. F.; Nogueira, N. C.; Rizzo, M. S.; Silva-Filho, E. C.; Costa, M. P.; Ribeiro, A. B.; *J. Drug Delivery Sci. Technol.* **2019**, *54*, 101306. [Crossref]
24. Silva, F. E. F.; Batista, K. A.; Di-Medeiros, M. C. B.; Silva, C. N. S.; Moreira, B. R.; Fernandes, K. F.; *Mater. Sci. Eng. C* **2016**, *58*, 927. [Crossref]
25. Ribeiro, I. S.; Pontes, F. J. G.; Carneiro, M. J. M.; Sousa, N. A.; Pinto, V. P. T.; Ribeiro, F. O. S.; Silva, D. A.; Araújo, G. S.; Marinho, J. D. B.; Araújo, A. J.; Paula, H. C. B.; Feitosa, J. P. A.; de Paula, R. C. M.; *Int. J. Biol. Macromol.* **2021**, *179*, 314. [Crossref]
26. Oliveira, A. C. J.; Chaves, L. L.; Ribeiro, F. O. S.; Lima, L. R. M.; Oliveira, T. C.; García-Villén, F.; Viseras, C.; de Paula, R. C. M.; Rolim-Neto, P. J.; Hallwass, F.; Silva-Filho, E. C.; Silva, D. A.; Soares-Sobrinho, J. L.; Soares, M. F. L. R.; *Carbohydr. Polym.* **2021**, *254*, 117226. [Crossref]
27. Richter, A. R.; Carneiro, M. J.; Sousa, N. A.; Pinto, V. P. T.; Freire, R. S.; Sousa, J. S.; Mendes, J. F. S.; Fontenelle, R. O. S.; Feitosa, J. P. A.; Paula, H. C. B.; Goycoolea, F. M.; de Paula, R. C. M.; *Int. J. Biol. Macromol.* **2020**, *152*, 492. [Crossref]
28. Lima, I.; Moreno, L.; Dias, S.; Silva, D.; Oliveira, AC; Soares, L.; Sousa, R.; Dittz, D.; Rolim, H.; Nunes, L.; *Carbohydr. Polym. Technol. Appl.* **2023**, *5*, 100265. [Crossref]
29. Oliveira, A. C. J.; Silva, E. B.; Oliveira, T. C.; Ribeiro, F. O. S.; Nadvorny, D.; Oliveira, J. W. F.; Borrego-Sánchez, A.; Rodrigues, K. A. F.; Silva, M. S.; Rolim-Neto, P. J.; Viseras, C.; Silva-Filho, E.C.; Silva, D. A.; Chaves, L. L.; Soares, M. F. L. R.; Soares-Sobrinho, J. L.; *Int. J. Biol. Macromol.* **2023**, *230*, 123272. [Crossref]
30. Maciel, J. S.; Azevedo, S.; Correia, C. R.; Costa, A. M. S.; Costa, R. R.; Magalhães, F. A.; Sousa, A. A. M.; Costa, J. F. G.; de Paula, R. C. M.; Feitosa, J. P. A.; Mano, J. F.; *Macromol. Mater. Eng.* **2019**, *304*, 1800574. [Crossref]
31. Ferreira, C. R. N.; Ramos, E. L. L.; Araujo, L. F. S.; Sousa, L. M. S.; Feitosa, J. P. A.; Cunha, A. F.; Oliveira, M.; Mano, J. F.; Maciel, J. S.; *Int. J. Biol. Macromol.* **2021**, *176*, 26. [Crossref]
32. de Paula, R. C. M.; Heatley, F.; Budd, P. M.; *Polym. Int.* **1998**, *45*, 27. [Crossref]
33. Menestrina, J. M.; Iacomini, M.; Jones, C.; Gorin, P. A. J.; *Phytochemistry* **1998**, *47*, 715. [Crossref]
34. Nypelö, T.; Berke, B.; Spirk, S.; Sirviö, J. A.; *Carbohydr. Polym.* **2021**, *252*, 117105. [Crossref]
35. Yin, H.; Song, P.; Chen, X.; Xiao, M.; Tang, L.; Huang, H.; *Biomacromolecules* **2022**, *23*, 253. [Crossref]
36. Kristiansen, K. A.; Potthast, A.; Christensen, B. E.; *Carbohydr. Res.* **2010**, *345*, 1264. [Crossref]
37. World Health Organization (WHO); *Global Cancer Observatory: Cancer Today*, https://gco.iarc.who.int/, accessed in May 2024.
38. Dwitya, S. S.; Lin, K. S.; Weng, M. T.; Mdlovu, N. V.; Tsai, W. C.; Wu, C. M.; *J. Ind. Eng. Chem.* **2024**, *129*, 499. [Crossref]
39. Oliveira, D. D. S.; Lapierre, T. J. W. J. D.; Silva, F. C.; Cunha, I. V.; Souza, R. A. C.; Matos, P. A.; Almeida, G. M.; Oliveira, C. G.; Araújo, T. G.; Tsubone, T. M.; Rezende Jr., C. O.; *J. Braz. Chem. Soc.* **2024**, *35*, e-20230128. [Crossref]
40. Misiak, P.; Niemirowicz-Laskowska, K.; Markiewicz, K. H.; Wielgat, P.; Kurowska, I.; Czarnomysy, R.; Misztalewska-Turkowicz, I.; Car, H.; Bielawski, K.; Wilczewska, A. Z.; *Cancer Nanotech.* **2023**, *14*, 23. [Crossref]
41. Farahani, B. V.; Behbahani, G. R.; Javadi, N.; *J. Braz. Chem. Soc.* **2016**, *27*, 694. [Crossref]
42. An, L.; Jia, Y.; Li, J.; Xiao, C.; *Int. J. Biol. Macromol.* **2023**, *233*, 123277. [Crossref]

43. Panda, P. K.; Jain, S. K.; *Int. J. Pharm. Investig.* **2023**, *13*, 87. [Crossref]
44. Henri, J. L.; Nakhjavani, M.; McCoombe, S.; Shigdar, S.; *Biochimie* **2023**, *204*, 108. [Crossref]
45. Wang, J.; Zhang, Y.; Zhang, G. P.; Xiang, L.; Pang, H. W.; Xiong, K.; Lu, Y.; Li, J. M.; Dai, J.; Lin, S.; Fu, S. Z.; *Drug Delivery* **2022**, *29*, 588. [Crossref]
46. Feng, X.; Li, D.; Han, J.; Zhuang, X.; Ding, J.; *Mater. Sci. Eng.: C* **2017**, *76*, 1121. [Crossref]
47. Fernandes, T. S.; Santos, E. C. S.; Madriaga, V. G. C.; Bessa, I. A. A.; Nascimento, V.; Garcia, F.; Ronconi, C. M.; *J. Braz. Chem. Soc.* **2019**, *30*, 2452. [Crossref]
48. Santos, E. C. S.; dos Santos, T. C.; Fernandes, T. S.; Jorge, F. L.; Nascimento, V.; Madriaga, V. G. C.; Cordeiro, P. S.; Checca, N. R.; da Costa, Pinto, N. M.; Ronconi, C. M.; *J. Mater. Chem. B* **2020**, *8*, 703. [Crossref]
49. Rodrigues, J. F.; de Paula, R. C. M.; Costa, S. M. O.; *Polímeros* **1993**, *16*, 31. [Crossref]
50. Zhao, H.; Heindel, N. D.; *Pharm. Res.* **1991**, *8*, 400. [Crossref]
51. Xu, W.; Ding, J.; Xiao, C.; Li, L.; Zhuang, X.; Chen, X.; *Biomaterials* **2015**, *54*, 72. [Crossref]
52. Li, D.; Han, J.; Ding, J.; Chen, L.; Chen, X.; *Carbohydr. Polym.* **2017**, *161*, 33. [Crossref]
53. Kalyanasundaram, K.; Thomas, J. K.; *J. Am. Chem. Soc.* **1977**, *99*, 2039. [Crossref]
54. Mosmann, T.; *J. lmmunol. Methods* **1983**, *65*, 55. [Crossref]
55. Berridge, M. V.; Tan, A. S.; McCoy, K. D.; Wang, R. U. I.; *Biochemica* **1996**, *4*, 14. [Link] accessed in May 2024
56. Radushev, D.; *GraphPad Prism*, version 5.0.3; GraphPad Software, USA, 2009.
57. *OriginPro*, version *8.5.0 SR1*; OriginLab Corporation, USA, 2010.
58. Neacșu, A.; *Thermochim. Acta* **2018**, *661*, 51. [Crossref]
59. Wang, Y.; Bai, F.; Luo, Q.; Wu, M.; Song, G.; Zhang, H.; Cao, J.; Wang, Y.; *Int. J. Biol. Macromol.* **2019**, *121*, 964. [Crossref]
60. Niu, L.; Zhu, F.; Li, B.; Zhao, L.; Liang, H.; Yan, Y.; Tan, H.; *Mater. Chem. Front.* **2018**, *2*, 1529. [Crossref]
61. Tian, H.; Yu, L.; Zhang, M.; He, J.; Sun, X.; Ni, P.; *Colloids Surf., B* **2023**, *228*, 113400. [Crossref]
62. Li, D.; Ding, J.; Zhuang, X.; Chen, L.; Chen, X.; *J. Mater. Chem. B* **2016**, *4*, 5167. [Crossref]
63. Wang, Y.; Yang, M.; Qian, J.; Xu, W.; Wang, J.; Hou, G.; Ji, L.; Suo, A.; *Carbohydr. Polym.* **2019**, *203*, 203. [Crossref]
64. Curcio, M.; Cirillo, G.; Paolì, A.; Naimo, G. D.; Mauro, L.; Amantea, D.; Leggio, A.; Nicoletta, F. P.; Iemma, F.; *Colloids Surf., B* **2020**, *185*, 110537. [Crossref]
65. Danaei, M.; Dehghankhold, M.; Ataei, S.; Hasanzadeh Davarani, F.; Javanmard, R.; Dokhani, A.; Khorasani, S.; Mozafari, M. R.; *Pharmaceutics* **2018**, *10*, 57. [Crossref]
66. Eaton, P.; Quaresma, P.; Soares, C.; Neves, C.; Almeida, M. P.; Pereira, E.; West, P.; *Ultramicroscopy* **2017**, *182*, 179. [Crossref]
67. Li, D.; Feng, X.; Chen, L.; Ding, J.; Chen, X.; *ACS Biomater. Sci. Eng.* **2018**, *4*, 539. [Crossref]
68. Zeng, L.; An, L.; Wu, X.; *J. Drug Delivery* **2011**, ID 370308. [Crossref]
69. Sagnella, S. M.; Duong, H.; Macmillan, A.; Boyer, C.; Whan, R.; McCarroll, J. A.; Davis, T. P.; Kavallaris, M.; *Biomacromolecules* **2014**, *15*, 262. [Crossref]
70. Guo, F.; Yu, N.; Jiao, Y.; Hong, W.; Zhou, K.; Ji, X.; Yuan, H.; Wang, H.; Li, A.; Wang, G.; Yang, G.; *Drug Delivery* **2021**, *28*, 1709. [Crossref]
71. Suffness, M.; Pezzuto, J. M.; *Methods in Plant Biochemistry: Assays for Bioactivity*, 6th ed.; Academic Press: London, UK, 1991.

Submitted: February 5, 2024
Published online: May 27, 2024